Oscillatory flow through submerged canopies: 2. Canopy mass transfer

Ryan J. Lowe, Jeffrey R. Koseff, and Stephen G. Monismith

Environmental Fluid Mechanics Laboratory, Department of Civil and Environmental Engineering, Stanford University, Stanford, California, USA

James L. Falter

Hawaii Institute of Marine Biology, University of Hawaii, Kaneohe, Hawaii, USA

Received 26 October 2004; revised 11 February 2005; accepted 25 May 2005; published 15 October 2005.

[1] Mass transfer rates from submerged canopies constructed from arrays of vertical cylinders were investigated for a range of different cylinder spacings under both unidirectional and oscillatory flow. Individual canopy elements made from gypsum were dissolved in fresh water to simulate the mass transfer of dissolved metabolites to and from canopies of living benthic organisms. Mass transfer rates under oscillatory flow were up to three times higher than values measured for a comparable unidirectional current. This enhancement was shown to be a strong function of the canopy element spacing. A model was developed to predict canopy mass transfer rates on the basis of the in-canopy flow speed and was generalized to incorporate either unidirectional or oscillatory flow. Agreement between the modeled and experimentally measured mass transfer rates indicate that enhanced mass transfer to/from living benthic canopies under oscillatory flow is driven primarily by the higher in-canopy water motion generated by the oscillatory flow, as detailed in the companion paper (Lowe et al., 2005).

Citation: Lowe, R. J., J. R. Koseff, S. G. Monismith, and J. L. Falter (2005), Oscillatory flow through submerged canopies: 2. Canopy mass transfer, *J. Geophys. Res.*, *110*, C10017, doi:10.1029/2004JC002789.

1. Introduction

[2] The exchange of dissolved metabolites (e.g., CO_2, O_2, NH_4^+, NO_3^-, and PO_4^{3-}) between benthic organisms and ambient water is essential for sustaining critical biological processes such as growth, photosynthesis, and respiration. The biological demand for and production of these metabolites can lead to the formation of concentration boundary layers adjacent to the active surfaces of these organisms. The thickness of these concentration boundary layers is primarily controlled by the physical interaction of the benthic organisms with water flowing past them. In general, increasing water motion decreases the thickness of the concentration boundary layers thereby increasing the maximum possible transfer of dissolved metabolites between the organism and the ambient water [*Sanford and Crawford*, 2000]. Prior work has shown that the demand for nutrients by, for example, coral reef [*Atkinson and Bilger*, 1992] and seagrass [*Thomas et al.*, 2000] communities is high enough such that the uptake of dissolved nutrients is entirely limited by their physical transfer across concentration boundary layers and, thus, controlled by the interaction of these benthic communities with their hydrodynamic environment. *Bilger and Atkinson* [1992] termed these conditions as being "mass transfer limited." Photosynthesis [*Patterson et al.*, 1991; *Lesser et al.*, 1994; *Carpenter et al.*, 1991], respiration [*Sebens et al.*, 2003], and nitrogen fixation [*Williams and Carpenter*, 1998] have also been shown to increase with increasing water motion, indicating some degree of mass transfer limitation on the rates of these processes as well.

[3] Most studies of the effect of water motion on the metabolism of benthic organisms have been conducted only under conditions of steady, unidirectional flow. However, many benthic communities live in shallow coastal environments (<20 m) where they are exposed to oscillatory flow generated by surface waves. Several studies have reported that rates of mass transfer to benthic communities under oscillatory flow are "enhanced" by factors ranging from 1.2 to 3, relative to rates measured under steady flow [*Carpenter et al.*, 1991; *Williams and Carpenter*, 1998; *Falter et al.*, 2005; *Reidenbach et al.*, 2005]. To date, the physical mechanisms responsible for this enhancement have not been identified and modeled.

[4] Benthic organisms often form very rough surfaces on the sea floor that can be described as submerged canopies. These canopies act to retard the exchange of mass and momentum between the overlying water column and the surfaces of the organisms located inside the canopy [*Finnigan*, 2000]. As an example, consider the *Porites compressa* coral colony in Figure 1 (a photo of a full *Porites compressa* pavement is given in the work of *Lowe*

0148-0227/05/2004JC002789$09.00

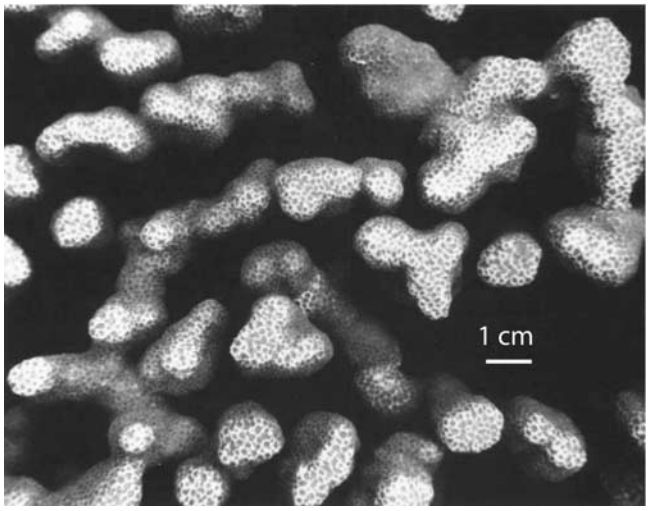

Figure 1. Image showing the branching structure of the coral *Porites compressa* (photo courtesy of M. Koehl). For a photo of a full *Porites compressa* pavement, see LKM1, Figure 1a. See color version of this figure in the HTML.

et al. [2005, Figure 1a]). Nutrient uptake at the coral surface involves the transfer of the nutrient from the water column into the canopy formed by the coral branches, where the nutrient can be assimilated. The preceding companion paper *Lowe et al.* [2005] (hereinafter referred to as LKM1), demonstrated using simplified, experimental canopies, that the in-canopy flow was much higher under oscillatory flow than under unidirectional flow. This was shown to be a direct result of the different momentum balance established inside the canopy for these different flows. Specifically, the results showed that the attenuation of the in-canopy flow could be predicted using three dimensionless parameters that were a function of wave kinematic and canopy geometry parameters.

[5] The purpose of this paper (Part 2) is to evaluate how rates of mass transfer to/from submerged canopies may differ with varying flow conditions and canopy geometries. This paper is notably different from previous scalar transport studies in canopy arrays [e.g., *Nepf*, 1999; *White and Nepf*, 2003], which focus on the dispersion of a scalar after it has been released inside the canopy. The focus of this study is specifically to understand how flow and canopy geometry controls the release rate (mass flux) at the canopy element surfaces (i.e., the solid-fluid boundary) under both unidirectional and oscillatory flow conditions. For unidirectional flow mass transfer from the surfaces of two-dimensional ridges has recently been investigated by *Barlow et al.* [2004] and *Harman et al.* [2004], however, to our knowledge the analogous problem of mass transfer from the surfaces formed by a three-dimensional array of canopy elements has not received attention. This paper builds upon results from LKM1, by first developing a model in section 2 for estimating mass transfer to/from submerged canopies that is valid under both unidirectional and oscillatory flow. Mass transfer rates from model canopies are then investigated through a series of experiments where individual canopy elements constructed of gypsum (plaster) are dissolved under various flow conditions and canopy element spacings.

2. Canopy Mass Transfer

[6] The model canopies used in these experiments are composed of a vertical array of circular cylinders that only occupy a small fraction of the water column, identical to the arrays used in the experiments described in the work of LKM1. However, in these mass transfer experiments, several plastic cylinders were replaced by solid gypsum cylinders. The dissolution of gypsum ($CaSO_4 \cdot 2H_2O$) has long been used as a means of describing water motion in aquatic environments (see *Porter et al.* [2000] for a review). It has also been used as a tool for studying the mass transfer characteristics of coral reef communities [*Baird and Atkinson*, 1997; *Falter et al.*, 2005; *Reidenbach et al.*, 2005]. This utility arises from the high solubility of gypsum in water. As a result, rates of gypsum dissolution are limited by the mass transfer of Ca^{2+} and SO_4^{2-} ions away from a gypsum surface and are therefore controlled by the interaction of the gypsum form with its flow environment.

[7] A simple model is now presented to predict mass transfer from a canopy as a function of canopy geometry and flow parameters. The approach first involves developing a model to predict mass transfer from a single element inside the canopy. This model is then extended to predict mass transfer from a full canopy consisting of an array of individual elements.

2.1. Mass Transfer From a Canopy Element

[8] For convective mass transfer problems it is customary to parameterize the rate of mass transfer of the solute (e.g., Ca^{2+} and SO_4^{2-} ions) at a point on a surface using the flux relation

$$F = \beta(C_o - C_{ref}), \tag{1}$$

where F is the molar mass flux [$mol\ m^{-2}\ s^{-1}$] at the surface, β is the mass transfer coefficient [$m\ s^{-1}$], and C_o and C_{ref} represent the concentrations [$mol\ m^{-3}$] of the solute at the surface and in the surrounding fluid, respectively. We first consider the case of mass transfer from a single cylindrical canopy element, where the subscript "e" will be used to denote mass transfer parameters associated with a canopy element. Owing to variations in the flow structure around the cylinder, the mass flux F_e and mass transfer coefficient β_e will, in general, vary with local position on the cylinder surface [*Zukauskas and Ziugzda*, 1985]. Since the model canopies used in these experiments consist of a vertical array of circular cylinders, a simple canopy mass transfer model can be developed based on previous studies which measured heat/mass transfer from circular cylinders in a cross flow. Several of these studies have presented empirical formulas to predict this rate of mass transfer. In many of these studies, convective mass transfer from a cylinder is parameterized in the following form:

$$Sh_e = f(Re_e, Sc), \tag{2}$$

where Sh_e is the Sherwood number, f is an empirical function, Re_e is the Reynolds number based on the cylinder

diameter d, and $Sc = \nu/D$ is the Schmidt number based on the diffusivity of the solute D. Here the Sherwood number Sh_e is defined as

$$Sh_e = \frac{\beta_e d}{D}. \quad (3)$$

Although several empirical functions f exist to predict mass transfer from a circular cylinder in a cross flow, the formula by *Churchill and Bernstein* [1977] is frequently cited. This formula is valid for a wide range of Re_e and Sc, but for the high values in our experiments (e.g., $Re_e > 100$ and $Sc > 100$) the *Churchill and Bernstein* [1977] formula reduces to the simple expression

$$Sh_e = f(Re_e, Sc) = 0.62 Re_e^{1/2} Sc^{1/3}. \quad (4)$$

It should be noted that Sh_e in equation (4) is based on the average mass transfer coefficient integrated over the circumference of the cylinder [*Churchill and Bernstein*, 1977].

[9] Equation (4) was developed from experiments where the cylinder was effectively infinitely long such that flow was uniform along the cylinder length, while the model canopy elements used in this study are of finite length. In the work of LKM1 the velocity field inside the canopy is shown to vary vertically, particularly near the top of the canopy where the greatest shear in the flow is present. Thus Sh_e is expected to vary along the length of a canopy element, with more mass transfer occurring at regions on the cylinder surface located near the top of the canopy where the local velocity is highest. To simplify the problem, only the canopy depth-averaged values of these mass transfer parameters are considered; this will be denoted by the "overhat" symbol. For example, a representative Sherwood number $\widehat{Sh_e}$ associated with a canopy element can be defined as the depth-averaged value of Sh_e, i.e.,

$$\widehat{Sh_e} = \frac{1}{h_c}\int_0^{h_c} Sh_e(z)dz, \quad (5)$$

where h_c is the height of the cylinder. Similarly a canopy depth-averaged mass flux $\widehat{F}_e$ and mass transfer coefficient $\widehat{\beta}_e$ can be defined such that the flux relation in equation (1) can be used to describe the canopy element mass transfer,

$$\widehat{F}_e = \widehat{\beta}_e\left(C_o - \widehat{C}\right), \quad (6)$$

where $\widehat{C}$ is the spatially averaged in-canopy concentration.

[10] A simple model is now developed to predict $\widehat{\beta}_e$ from a single element in the canopy. For a cylinder in a cross flow, the mass transfer formula given in equation (4) is parameterized by the free-stream velocity away from the cylinder in the form of a Reynolds number. In our model we assume that mass transfer from a canopy element is described by the same formula, but that the appropriate velocity scale is the "in-canopy" velocity since this roughly represents the velocity around the cylinder surface. However, the mass transfer formula in equation (4) describes mass transfer from a cylinder in isolation. It is possible that spatial heterogeneities in the in-canopy velocity field and turbulence generated by upstream canopy elements will significantly modify the mass transfer processes. The applicability of this mass transfer formula to these canopy flows will be investigated using the experiments below.

[11] To simplify the mass transfer model we assume that the in-canopy velocity field is described by a single representative velocity $\widehat{U}_s$ equal to the canopy depth-averaged "flow speed". In an alternative approach we could have calculated $Sh_e(z)$ at each height based on the local velocity at that height and directly applied equation (5) to predict $\widehat{\beta}_e$. However, we compared the values of $\widehat{\beta}_e$ calculated using these different methods, and in our experiments the results agreed within the margin of error in the measurements. Therefore for convenience in this study we decided to apply the mass transfer model using a representative flow speed $\widehat{U}_s$. Following the notation in the work of LKM1, for a unidirectional current this flow speed $\widehat{U}_s$ is equal to the vertically averaged in-canopy velocity $\widehat{U}_c$. Although the mass transfer model presented here is based on a formula derived for unidirectional flow (equation (4)), it is extended to oscillatory flow conditions by using the average flow speed (over a wave period) of the oscillatory motion. At present this assumption is not automatically justified, but will be checked in the experiments described below. For oscillatory flow that is purely sinusoidal (e.g., linear waves), the average in-canopy flow speed $\widehat{U}_s$ is approximately equal to the root mean squared (rms) in-canopy velocity $\widehat{U}_w^{rms}$ defined in the work of LKM1 according to $\widehat{U}_s \approx 0.90\widehat{U}_w^{rms}$ [e.g., *Falter et al.*, 2005]. Therefore the rms flow speed can be assumed to be equal to the average flow speed without inducing a significant error.

[12] Given a value of $\widehat{U}_s$ based on either unidirectional and/or oscillatory flow conditions, the representative Sherwood number Sh_e can be estimated as

$$\widehat{Sh_e} = f\left(\widehat{Re_e}, Sc\right), \quad (7)$$

where the function f is given by equation (4) and $\widehat{Re_e}$ is a Reynolds number defined based on the representative in-canopy flow speed

$$\widehat{Re_e} = \frac{\widehat{U}_s d}{\nu}. \quad (8)$$

An apparent shortcoming of the model in equation (7) is that it can only accurately predict mass transfer from the circumferential surface area of a cylinder, and thus cannot accurately predict mass transfer occurring at the top. Rather than completely ignore mass transfer at the cylinder top, we assume that to a first approximation the local mass transfer coefficient at the cylinder top is approximately equal to the average coefficient $\widehat{\beta}_e$ calculated for the circumferential area using equation (4). The rate of mass transfer from the cylinder is then assumed to be $\widehat{F}_e A_e$, where A_e is the total exposed surface area (circumferential area plus top area). This approximation should be particularly accurate for canopies where the circumferential area is significantly

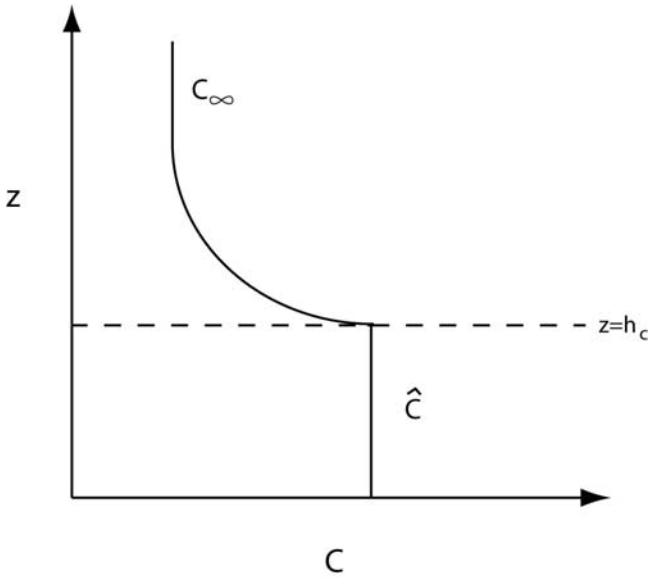

Figure 2. Simplified form of the concentration profile within and above the canopy, used in the canopy mass transfer model. The dashed line at $z = h_c$ denotes the height of the canopy.

larger than the top area, e.g., when $h_c/d > 1$. For example, in this study where $h_c/d = 2$ the top area of the cylinders comprises only 10% of the total exposed surface area.

[13] To apply this model, the in-canopy flow speed $\widehat{U}_s$ must be known, either by direct measurement or by relating $\widehat{U}_s$ to the velocity measured above the canopy as follows. In the work of LKM1 a model was presented to predict the canopy flow attenuation parameter, defined as the ratio of the in-canopy velocity to the above-canopy velocity. For unidirectional flow the attenuation parameter α_c was defined as

$$\alpha_c \equiv \frac{\widehat{U}_c}{U_{\infty,c}}, \tag{9}$$

where $U_{\infty,c}$ is the free stream velocity of the current. For an oscillatory flow the attenuation parameter α_w was defined as

$$\alpha_w \equiv \frac{\widehat{U}_w^{rms}}{U_{\infty,w}^{rms}}, \tag{10}$$

where $U_{\infty,w}^{rms}$ is the rms free-stream oscillatory flow velocity. Thus, given the above-canopy flow conditions and an estimate of either α_c or α_w, the representative canopy flow speed $\widehat{U}_s$ can be estimated for use in predicting $\widehat{\beta}_e$.

2.2. Mass Transfer From a Canopy Array

[14] In the previous section, mass transfer from a single element in the canopy was discussed, but it is ultimately desirable to predict mass transfer from a full canopy array. The single canopy element model is now extended to predict mass transfer from an array of canopy elements.

[15] In the simple canopy mass transfer model considered here, the concentration field is assumed to have the form given in Figure 2, where the in-canopy concentration $\widehat{C}$ is characterized by single representative value and the above-canopy concentration profile approaches a value C_∞ associated with the bulk fluid in the water column. Figure 3 shows a plan view of a model canopy used in the experiments. The dashed box denotes a repeating canopy element unit, having a plan area $A_T = (S + d)^2$ based on the cylinder spacing S. A mass transfer coefficient β_{can} associated with the canopy array can be defined, as was done for a canopy element in equation (1), i.e.,

$$F_{can} = \beta_{can}(C_o - C_\infty). \tag{11}$$

In this case, F_{can} is the mass flux of the scalar from inside the canopy to the overlying water column, and C_o and C_∞ represent the concentrations of the solute at the canopy element surface and the water column, respectively. Note that C_o is used in equation (11) rather than $\widehat{C}$, since C_o is a known parameter. The canopy mass flux F_{can} thus represents the rate at which mass is exchanged from the canopy element surfaces to the above canopy flow per unit total canopy plan area.

[16] The concentration C_o in equation (11) is identical to that in equation (1) since it is, by definition, the concentration at the canopy element surface. However, the concentration C_∞ in equation (11) is not necessarily equal to $\widehat{C}$ in equation (1). This discrepancy results from the fact that a dissolved compound released within a canopy can be trapped inside the canopy and advected downstream [see *Nepf and Vivoni*, 2000]. As a result, even when C_∞ above the canopy does not vary with downstream distance, the

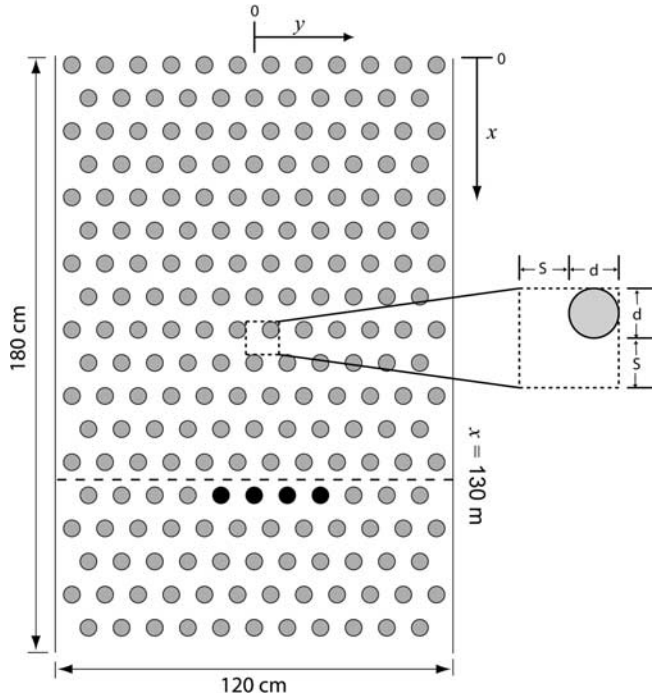

Figure 3. Cylinder array layout for experiments with spacing $S = 5$ cm. The dashed box indicates a repeating canopy unit of plan area $A_T = (S + d)^2$. The black cylinders denote locations of gypsum canopy elements used to measure mass transfer.

concentration inside the canopy $\widehat{C}(x)$ can increase downstream as the dissolved compound is released into the canopy by upstream elements. This can reduce the concentration gradient at downstream canopy element surfaces, and thus effectively decrease $\widehat{\beta}_e$ associated with downstream elements. At some distance downstream, $\widehat{C}$ will attain a constant maximum value $\widehat{C}_{\max}$ when the mass transfer rate out at the top of the canopy equals the rate of scalar released by the canopy elements. In many circumstances both the maximum downstream concentration $\widehat{C}_{\max}$ and the water column concentration C_∞ are much smaller than C_o, and for this case the problem is greatly simplified since $\widehat{C}$ and C_∞ can effectively be ignored. Appendix A shows that this simplification can be assumed when $U_E/\beta_{can} \gg 1$, where U_E is a vertical canopy exchange velocity. In other words, this assumption is valid when the vertical exchange velocity which transports the scalar out of the canopy is much larger than the rate at which the scalar is released into the canopy by the canopy elements. This simplification (ignoring $\widehat{C}$ and C_∞) is shown in Appendix A to be valid in all of the experiments described in this paper, as well as in many other practical problems of interest.

[17] For cases where the in-canopy concentration is fully developed, the total mass exchanged per unit time out of a repeating canopy unit into the water column is balanced by the mass released per unit time from a canopy element surface, i.e.,

$$F_{can}A_T = \widehat{F}_e A_e, \tag{12}$$

where A_e is the surface area of the canopy element. The total exposed surface area of a cylindrical canopy element used in these experiments is equal to the circumferential area plus the area at the top of the cylinder, i.e.,

$$A_e = \pi d h_c + 1/4\pi d^2. \tag{13}$$

Substituting equations (6) and (11) into equation (12) gives

$$\beta_{can}(C_o - C_\infty)A_T = \widehat{\beta}_e\left(C_o - \widehat{C}\right)A_e. \tag{14}$$

However, in Appendix A it is shown that $\widehat{C} \ll C_o$ and $C_\infty \ll C_o$ so equation (14) simplifies to

$$\frac{\beta_{can}}{\widehat{\beta}_e} \approx \frac{A_e}{A_T} = \pi\lambda_f + \lambda_p, \tag{15}$$

where the "lambda" parameters are defined as in the work of LKM1, i.e.,

$$\lambda_f = h_c d/(S+d)^2 \tag{16}$$

is the ratio of the cylinder frontal area to the total canopy plan area and

$$\lambda_p = \left(\pi d^2/4\right)/(S+d)^2 \tag{17}$$

is the ratio of plan area of a canopy element to the total canopy plan area. The canopy mass transfer coefficient β_{can} is shown in equation (15) to be related to $\widehat{\beta}_e$ simply by the canopy geometry parameters λ_f and λ_p. Finally, combining equation (15) with the mass transfer model in equation (7) gives an expression governing the canopy mass transfer coefficient

$$\beta_{can} = \frac{D}{d} f\left(\widehat{Re}_e, Sc\right) g\left(\lambda_f, \lambda_p\right), \tag{18}$$

where the function g is given in equation (15), i.e.,

$$g\left(\lambda_f, \lambda_p\right) \equiv \pi\lambda_f + \lambda_p. \tag{19}$$

Equation (18) shows that the canopy mass transfer coefficient β_{can} is a function of the in-canopy velocity (described by the function f) and the canopy geometry (described by the function g). For a given canopy consisting of elements having a fixed height h_c and diameter d, the functions f and g in equation (18) make opposing contributions to mass transfer as the spacing S of the canopy elements changes. For example, as the spacing S decreases, we see from equation (19) that the function g increases which results in higher mass transfer from the canopy due to the increase in the total canopy surface area. However, in the work of LKM1 it was shown that for a given above-canopy flow, the flow inside the canopy decreases as the spacing S decreases, so according to equation (7), this causes the function f to decrease which reduces the mass transfer coefficient β_{can}.

3. Experimental Methodology

3.1. Mass Transfer Measurements

[18] The experiments were conducted using the same model canopies described in the work of LKM1, i.e., we used individual cylinders with diameters d = 5 cm and height h_c = 10 cm, and cylinder spacings of S = 5, 10, and 15 cm. During all experiments the water depth was 43 cm. To measure rates of mass transfer from the canopy elements, a lateral row of four gypsum cylinders made from US Gypsum No. 1 Pottery Plaster was used in the canopy array [see LKM1, Figure 1b]. An analysis of this specific plaster by *Baird and Atkinson* [1997] showed that, by weight, it consists of greater than 96% $CaSO_4 \cdot 1/2H_2O$. Each gypsum cylinder was prepared as follows. For every 100 parts (by weight) of dry plaster used, 70 parts water was added. The plaster was stirred for 5 minutes and poured into a PVC pipe mold. Each gypsum cylinder was removed from its molding and dried at 50°C in a food dehydrator for 24 hours, which was found to be a sufficient time to remove all excess water. The initial dry weight (approximately 240 g) of each gypsum cylinder was then weighed to an accuracy of 0.1 g using a digital scale.

[19] Prior to each experiment, a lateral row of four PVC cylinders was removed from a row located a distance $x \approx$ 130 cm from the leading edge of the canopy and replaced by gypsum cylinder molds (Figure 3). To begin an experiment, the flume and/or wavemaker was turned on and allowed to run for 10 hours, during which the mass of a gypsum cylinder decreased by 1% to 4% of its original mass. During an experiment water temperature was recorded at the beginning and end of the experiment, since gypsum dissolution rates are weakly affected by water temperature

[*Thompson and Glenn*, 1994]. After 10 hours, the flow was stopped and the flume was drained. The four gypsum cylinders were then removed from the plates and were dried in the food dehydrator for at least 24 hours at 50°C, until all water was removed. Finally, each cylinder was reweighed giving a measure of the total mass loss during the experiment $\Delta M'$.

[20] During the flume filling and draining process, which each took approximately 30 minutes, some dissolution of the gypsum molds occurred as water flowed in and out of the flume. To quantify this concomitant mass loss, we performed three control experiments, each using a different cylinder spacing, in which the flume was filled and then immediately drained without ever turning on the wavemaker. In these control experiments, the mass loss from each gypsum cylinder averaged 0.4 ± 0.2 g. Therefore in all experiments 0.4 g was subtracted from the measured mass loss $\Delta M'$, since this mass reduction was not caused by the particular flow used in the experiments. The mass lost, which resulted only from the 10 hour flow, will be denoted ΔM, i.e., $\Delta M = \Delta M' - 0.4$ g.

[21] Mass transfer coefficients $\widehat{\beta}_e$ for each gypsum cylinder were calculated from the molar calcium flux and the calcium ion surface concentration $[Ca^{2+}]_o$ according to equation (6), i.e.,

$$\widehat{\beta}_e = \frac{\widehat{F}_e}{[Ca^{2+}]_o}, \tag{20}$$

where it is assumed that $\widehat{C} \ll C_o$ since the gypsum concentration is expected to be negligible inside the canopy (see Appendix A). The surface concentration $[Ca^{2+}]_o$ was calculated from the solubility of $CaSO_4$ in water [*Porter et al.*, 2000] using data from *Lide* [2003]. Since the temperature varied between just 15° and 17° C during the experiments, $[Ca^{2+}]_o$ was taken at the mean experimental temperature of 16°C and therefore assumed to have a constant value of 14.5 mol m^{-3} [*Lide*, 2003]. The solubility of $CaSO_4$ is only a weak function of temperature, so using a constant value of $[Ca^{2+}]_o$ will induce at most a 1% error. The mass flux $\widehat{F}_e$ was calculated from the mass loss from each gypsum cylinder according to

$$\widehat{F}_e = \frac{\Delta M}{W_g A_e \Delta t}, \tag{21}$$

where $W_g = 172.2$ g is the molecular weight of gypsum, $A_e = 1.65 \times 10^{-2}$ m^2 is the total surface area of a cylinder, and Δt is the duration of each experiment (~10 hours). Owing to the small decrease in the mass of the cylinders during the experiments (<4%), the change in surface area was negligible so A_s was assumed constant.

[22] In order to apply the canopy mass transfer model in equation (7), the Schmidt number Sc must be specified. It is thus necessary to determine the kinematic viscosity ν of the flume water as well as an effective diffusion coefficient D_{CaSO4} for the mass transfer process. Since the water temperature varied minimally during the experiments and averaged 16°C, a constant value $\nu = 1.1 \times 10^{-6}$ $m^2 s^{-1}$ was assumed. Mass and charge balance require that the mass fluxes of Ca^{2+} and SO_4^{2-} ions be equal, however, the diffusivities of Ca^{2+} and SO_4^{2-} in fresh water are not equal ($D_{Ca} = 6.4 \times 10^{-10}$ m^2 s^{-1} and $D_{SO4} = 8.6 \times 10^{-10}$ $m^2 s^{-1}$, respectively at 16°C; *Li and Gregory* [1974]). For two-ion electrolytes diffusing from high to low concentration, an effective diffusivity can be calculated from the weighted average of each constituent ion's free diffusivity [*Lerman*, 1979]:

$$D_{CaSO_4} = \frac{(|z^+| + |z^-|) D_{Ca} D_{SO4}}{|z^+| D_{Ca} + |z^-| D_{SO4}}, \tag{22}$$

where $z^+ = +2$ and $z^- = -2$ are the charge of the calcium and sulfate ions, respectively. This equation accounts for the attractive force exerted by the faster diffusing anion on the slower diffusing cation. In a freshwater solution containing dissolved $CaSO_4$, less than 1% of the total dissolved mass will form the ion pair $CaSO4^0$ [*Stumm and Morgan*, 1996]. Therefore >99% of the dissolved $CaSO_4$ will diffuse as free ions. For free Ca^{2+} and SO_4^{2-} diffusing from the gypsum surface, the effective diffusivity D_{CaSO4} of both species is $7.3 \pm 0.5 \times 10^{-10}$ $m^2 s^{-1}$, where the stated uncertainty is estimated from *Li and Gregory* [1974]. These values for ν and D_{CaSO4} give a value of $Sc = 1510$ which was assumed to be constant for all experiments.

3.2. Flow Measurements

[23] Full velocity profiles were not measured within and above the canopy, as were done in the work of LKM1. Instead, for each experiment the velocity was measured at a single height $z/h_c = 2.5$ using the Laser Doppler Anemometry (LDA) system described in the work of LKM1. The velocity profiles were then inferred from the profiles described in the work of LKM1, since flow in the flume was repeatable. The in-canopy velocity $\widehat{U}_s$ used in the mass transfer model (equation (7)) can then be calculated from the values of the canopy attenuation parameter (α_c or α_w) measured in the work of LKM1. A total of 9 unidirectional flow experiments (U1–U9), listed in Table 1, and 6 wave experiments (W1–W6), listed in 2, were conducted. For each wave experiment a weak background current was required to minimize the upstream reflection of wave energy. Following the notation used in the work of LKM1, for this combined wave-current flow case, the velocity field U is decomposed as

$$U(z,t) = U_c(z) + U_w(z,t), \tag{23}$$

where U_c is the "steady" component of the velocity field associated with the current and U_w is the "unsteady" component of the velocity field associated with the oscillatory flow.

4. Results

[24] For each unidirectional flow experiment, the mean value of ΔM from the four cylinders is listed in Tables 1 and 2. Results from the unidirectional and oscillatory flow experiments are now discussed separately.

4.1. Unidirectional Flow

[25] The 9 unidirectional flow experiments used three flow velocities and three cylinder spacings (Table 1). For

Table 1. Parameters for the Unidirectional Flow Experiments

Experiment	S, cm	$U_{\infty,c}$, cm/s	$\widehat{U}_c$, cm/s	ΔM, g	$\widehat{\beta}_e$, m/s $\times 10^{-6}$	β_{can}, m/s $\times 10^{-6}$
U1	5	5.0	0.6	2.9	1.9	3.3
U2	5	9.4	1.0	4.1	2.7	4.9
U3	5	15.6	1.7	6.3	4.2	7.4
U4	10	5.1	1.2	3.9	2.6	2.0
U5	10	9.3	2.1	6.0	4.0	3.1
U6	10	14.4	3.3	8.2	5.5	4.3
U7	15	4.9	1.7	4.1	2.8	1.3
U8	15	8.9	3.0	6.2	4.4	2.0
U9	15	13.9	4.7	9.3	6.4	2.9

each experiment, the average mass loss ΔM was used with equations (20) and (21) to calculate the canopy element mass transfer coefficient $\widehat{\beta}_e$ (Table 1). Figure 4 shows $\widehat{\beta}_e$ plotted as a function of the free-stream current velocity $U_{\infty,c}$, for the three cylinder spacings S/d = 1, 2 and 3. At each element spacing, $\widehat{\beta}_e$ increases as $U_{\infty,c}$ increases. Figure 4 further shows that for a fixed value of $U_{\infty,c}$, $\widehat{\beta}_e$ increases as the spacing S increases, confirming that mass transfer from a canopy element is a strong function of the canopy morphology.

[26] The canopy element mass transfer model in section 2 assumed that mass transfer is a function of the in-canopy flow speed, which for unidirectional flow is $\widehat{U}_s = \widehat{U}_c$. Given $\widehat{U}_s$, a value for $\widehat{Re}_e$ was then calculated using equation (8). In Figure 5, $\widehat{\beta}_e$ is plotted versus $\widehat{Re}_e$ and shows that mass transfer from a canopy element is indeed correlated with in-canopy water motion, since this collapses the data in Figure 4 onto a single curve that incorporates both the effect of the above-canopy flow and the canopy geometry. To check the mass transfer curve predicted from the model, equations (3) and (7) were used to predict $\widehat{\beta}_e$ for the range of $\widehat{Re}_e$ used in the experiments. Figure 5 shows the predicted curve as a solid line with the 95% confidence limits indicated. Measured $\widehat{\beta}_e$ are slightly higher than the predicted values, although near the upper confidence limit. This discrepancy could simply be the result of uncertainties in $[Ca^{2+}]_\circ$, uncertainties in the calculated diffusivity D_{CaSO4}, the way in which mass transfer at the tops of the cylinders was modelled, or even the mass transfer formula itself (equation (4)). Nevertheless, there is still good agreement between predicted and measured $\widehat{\beta}_e$ indicating that the mass transfer model works well to estimate canopy mass transfer rates for these flow conditions and canopy types.

[27] Having measured $\widehat{\beta}_e$, a canopy mass transfer coefficient β_{can} can be calculated using equation (15) (Table 1). Figure 6 shows β_{can} plotted as a function of the free-stream current velocity $U_{\infty,c}$, for the three cylinder spacings used. As expected, for a given canopy, β_{can} increases as $U_{\infty,c}$ increases. However, for a fixed flow velocity, Figure 6 shows that β_{can} increases as the canopy spacing S decreases. Therefore for the range of spacings used in these experiments, mass transfer from the canopy array was highest when the elements were most densely packed together since there were more canopy elements (and hence a larger exposed canopy element surface area) per unit total canopy plan area. This is opposite from the effect of canopy element spacing on $\widehat{\beta}_e$ (Figure 4). In this case, as the canopy density increased, β_e decreased due to the resulting weaker in-canopy flow caused by sheltering from upstream elements.

4.2. Oscillatory Flow

[28] Six oscillatory flow experiments (W1–W6) were conducted (Table 2). As discussed above, in all of these experiments a background current was required, so the velocity field was decomposed into a unidirectional U_c and oscillatory U_w component per equation (23). Table 2 lists the free-stream current velocity $U_{\infty,c}$ and oscillatory flow velocity $U^{rms}_{\infty,w}$ for each experiment.

[29] Values of $\widehat{\beta}_e$ were calculated for each oscillatory flow experiment using equations (20) and (21) (Table 2). Figure 5 shows $\widehat{\beta}_e$ plotted versus $\widehat{Re}_e$, where $\widehat{Re}_e$ is defined in equation (8) based on the in-canopy flow speed $\widehat{U}_s$. For these oscillatory flow experiments $\widehat{U}_s$ is thus composed of a unidirectional and oscillatory flow component, i.e., $\widehat{U}_s = \widehat{U}_c + \widehat{U}^{rms}_w$. Notably, $\widehat{\beta}_e$ measured for these oscillatory flow experiments is consistent with $\widehat{\beta}_e$ measured for the same values of $\widehat{Re}_e$ under unidirectional flow, suggesting that the in-canopy flow speed can be used to estimate canopy mass transfer under both oscillatory and unidirectional flow conditions. Evaluation of the data collected for all unidirectional and oscillatory flow experiments shows that measured values of $\widehat{\beta}_e$ are slightly higher than the predicted curve obtained from the canopy mass transfer model, as shown in Figure 5, although near the upper confidence limit. The dashed line in Figure 5 represents the curve obtained by fitting

Table 2. Parameters for the Wave Experiments

Experiment	S, cm	T, s	$U_{\infty,c}$, cm/s	$\widehat{U}_c$, cm/s	$U^{rms}_{\infty,w}$, cm/s	$\widehat{U}^{rms}_w$, cm/s	ΔM, g	$\widehat{\beta}_e$, m/s $\times 10^{-6}$	β_{can}, m/s $\times 10^{-6}$
W1	5	2.0	5.0	0.6	4.8	3.4	10.5	6.9	12.3
W2	5	3.0	5.9	0.6	2.9	2.1	7.8	5.2	9.2
W3	10	2.0	5.8	1.4	4.0	3.5	10.7	7.3	5.7
W4	10	3.0	5.4	1.3	2.2	2.0	8.0	5.4	4.2
W5	15	2.0	5.0	1.7	4.6	4.3	10.1	7.2	3.3
W6	15	3.0	5.2	1.8	2.8	2.6	8.1	5.6	2.6

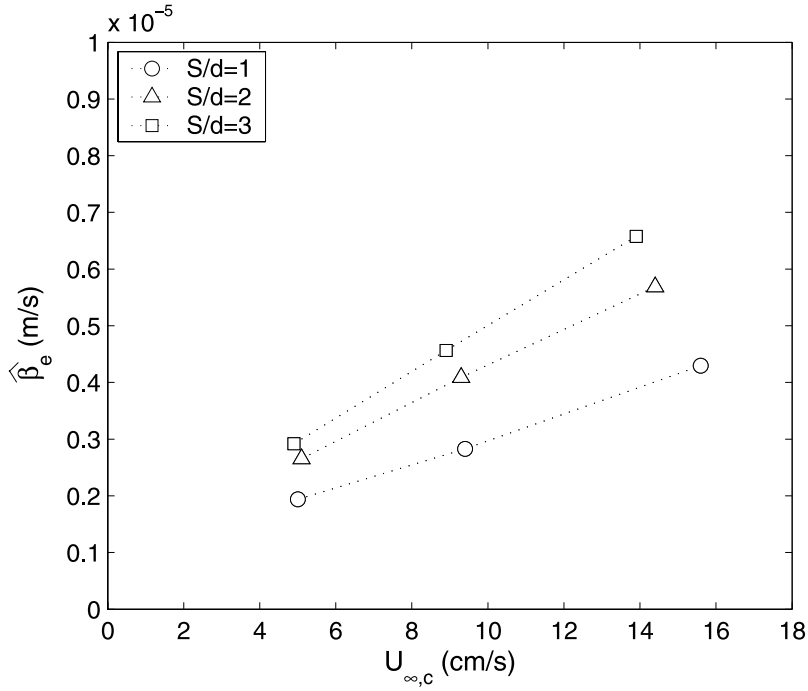

Figure 4. Canopy element mass transfer coefficient $\widehat{\beta}_e$ as a function of the unidirectional free-stream velocity $U_{\infty,c}$ for each cylinder spacing S.

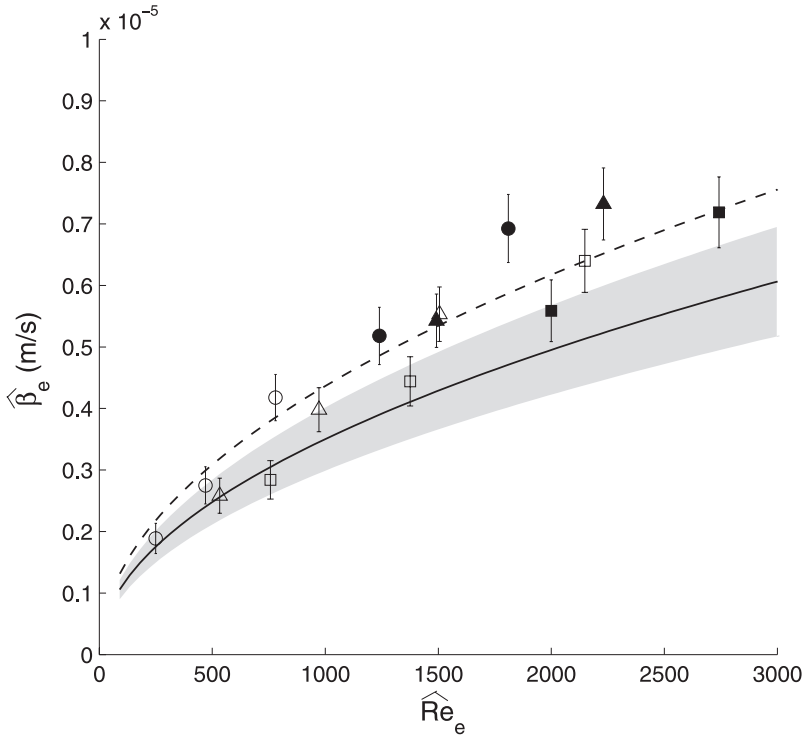

Figure 5. Measured mass transfer coefficient $\widehat{\beta}_e$ plotted versus the in-canopy Reynolds number $\widehat{Re}_e$. Open symbols denote unidirectional experiments (U1–U9). Closed symbols denote oscillatory experiments (W1–W6). Symbols represent canopy element spacing: circles, S/d = 1; triangles, S/d = 2; squares, S/d = 3. Predicted curve from the mass transfer model is shown as a solid line (gray region denotes 95% confidence limits). Dashed line corresponds to fitted curve $\widehat{Sh}_e/Sc^{1/3} = 0.82\widehat{Re}_e^{1/2}$.

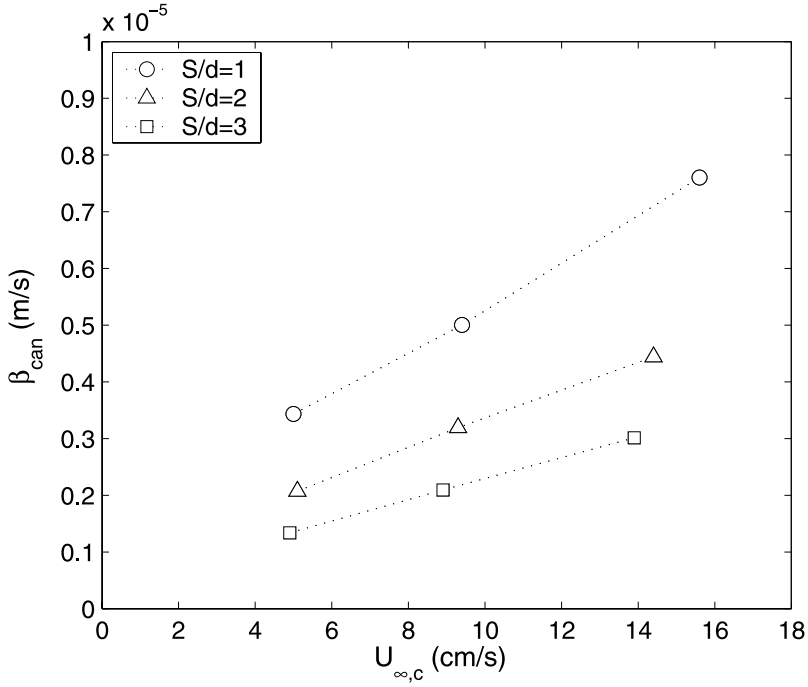

Figure 6. Canopy array mass transfer coefficient β_{can} versus the unidirectional free-stream velocity $U_{\infty,c}$, for each cylinder spacing S.

the function $a\widehat{Re}_e^{1/2}$ to the data, where a is a fitting coefficient. The best fit gives $\widehat{Sh}_e = (0.82 \pm 0.05)\widehat{Re}_e^{1/2}Sc^{1/3}$ and comparison with equation (4) shows that this coefficient is slightly larger, although similar, to the value 0.62 suggested by *Churchill and Bernstein* [1977].

[30] Although these results show that unidirectional and oscillatory flow produce the same canopy mass transfer rates when the in-canopy flow speeds are matched, in practice mass transfer rates are generally related to the above-canopy water motion. To compare differences in mass transfer between the unidirectional and oscillatory flow experiments, each measured mass transfer coefficient is normalized by its corresponding above-canopy velocity to produce a nondimensional parameter called a Stanton number [*Kays and Crawford*, 1993]. For unidirectional flow the Stanton number St_c is defined based on the free-stream velocity $U_{\infty,c}$:

$$St_c = \frac{\widehat{\beta}_e}{U_{\infty,c}}. \tag{24}$$

Similarly, for "pure" oscillatory flow (no current) the Stanton number St_w is defined based on the free stream rms oscillatory flow velocity $U_{\infty,w}^{rms}$, since for sinusoidal flow the rms velocity is approximately equal to the average flow speed over a wave period (see discussion in section 2):

$$St_w = \frac{\widehat{\beta}_e}{U_{\infty,w}^{rms}}. \tag{25}$$

To compare differences in mass transfer resulting from unidirectional and oscillatory flow, a "mass transfer enhancement factor" is defined as

$$E \equiv \frac{St_w}{St_c} \tag{26}$$

such that when E is greater than 1, an oscillatory flow induces higher mass transfer compared to a unidirectional flow of the same magnitude [*Falter et al.*, 2005]. The Stanton number in equation (25), however, is defined based on pure oscillatory flow, while in the oscillatory flow experiments a weak background current was always present. To isolate the mass transfer resulting from only the oscillatory component of flow, to an approximation it is assumed that the total mass transfer is the sum of unidirectional and oscillatory flow contributions. The estimated contribution of the current on mass transfer is then removed by assuming that its contribution can be determined from the fitted mass transfer relation $\widehat{Sh}_e = 0.82\widehat{Re}_e^{1/2}Sc^{1/3}$ using the measured $\widehat{U}_c$. Figure 7 shows E plotted versus the canopy element spacing S/d, where each data point represents the average value of E at the given spacing. Figure 7 shows that, in general, E is significantly greater than one indicating that an oscillatory flow can greatly enhance mass transfer from a canopy. The degree of this enhancement varies according to the canopy element spacing, and ranges from about 3 times higher in experiments with S/d = 1, to 1.5 times higher in experiments with S/d = 3. Thus the mass transfer enhancement becomes more pronounced as the canopies become more dense.

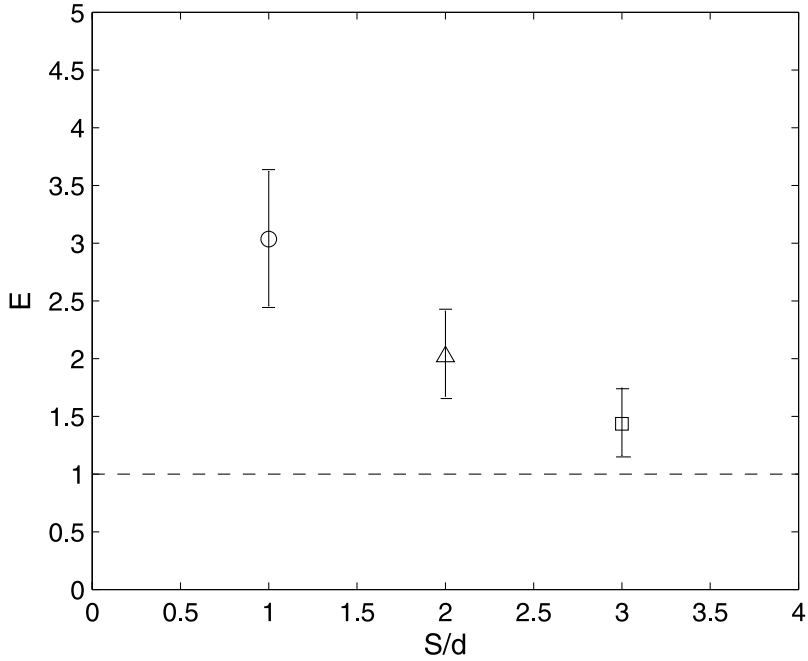

Figure 7. Enhancement of mass transfer E resulting from oscillatory flow over unidirectional flow, calculated based on the above-canopy flow speed, as a function of the canopy element spacing S. Each point represents the average of E at a spacing and the error bars denote the 95% confidence limits.

[31] In general, the magnitude of the enhancement for a given canopy is expected to be a function of both the canopy geometry and the oscillatory flow conditions. On the basis of the definition of E in equation (26), it can be shown that due to the correlation of canopy mass transfer with $\widehat{Re}_e^{1/2}$ in equation (4),

$$E = \left(\frac{\alpha_w}{\alpha_c}\right)^{1/2}, \tag{27}$$

where α_c and α_w are the attenuation parameters associated with unidirectional and oscillatory flows, respectively, as defined in equations (9) and (10). For a given canopy, it was shown in the work of LKM1 that α_w decreases as the orbital excursion length of the oscillatory flow A_∞^{rms} increases. For canopies with $S/d = 1$, 2 and 3, α_w was calculated by LKM1 as a function of A_∞^{rms} [see LKM1, Figure 4]. These curves can be used in conjunction with equation (27) to calculate theoretical curves of E for the canopies used in these mass transfer experiments. At each spacing, Figure 8 shows that E approaches 1 as the orbital excursion length A_∞^{rms} increases. This is expected since, as A_∞^{rms} increases, α_w approaches the unidirectional value α_c, and thus $E = 1$ per equation (27). Alternatively, for small A_∞^{rms} LKM1 showed that α_w approaches a maximum limit α_i where the flow is dominated by the canopy inertia force. Therefore, as A_∞^{rms} is reduced, a maximum value of E is attained, which is observed in Figure 8. This maximum value $E_{\max}$ can be estimated as

$$E_{\max} = \left(\frac{\alpha_i}{\alpha_c}\right)^{1/2}, \tag{28}$$

where expressions to estimate α_i and α_c are given in the work of LKM1 (see their equations (24) and (26)). Figure 8 shows that $E_{\max}$ increases as the canopy element spacing decreases, consistent with enhancement trend observed in Figure 7. This is because the ratio α_i/α_c increases as the canopies become more dense. Note that there is a discrepancy between the range of E predicted in Figure 8 ($\sim$1.7 to $\sim$2.6) compared to the values measured in the experiments ($\sim$1.4 to $\sim$3.0). This discrepancy, however, is comparable to the relatively large uncertainty in measured E and is also at least partially due to the fact that the predicted E curves are derived using the canopy flow model described in LKM1, where some disparity existed between the predicted and observed in-canopy flow.

5. Discussion and Conclusions

[32] Results from these experiments indicate that mass transfer from submerged canopies is controlled by the in-canopy flow speed. In the work of LKM1 it was shown that an oscillatory flow always produces higher in-canopy flow when compared to a unidirectional current of the same magnitude. As a consequence, mass transfer rates are enhanced when the flow is oscillatory. In our experiments, mass transfer rates normalized by the magnitude of the above-canopy flow were measured to be 1.5 to 3 times higher when the flow was oscillatory. These results stress the importance of directly measuring flow inside a canopy when trying to relate flow effects to mass transfer processes. Simply measuring the flow above the canopy to infer canopy mass transfer processes such as nutrient uptake is insufficient, since mass transfer is ultimately governed by the in-canopy water motion which strongly depends on the

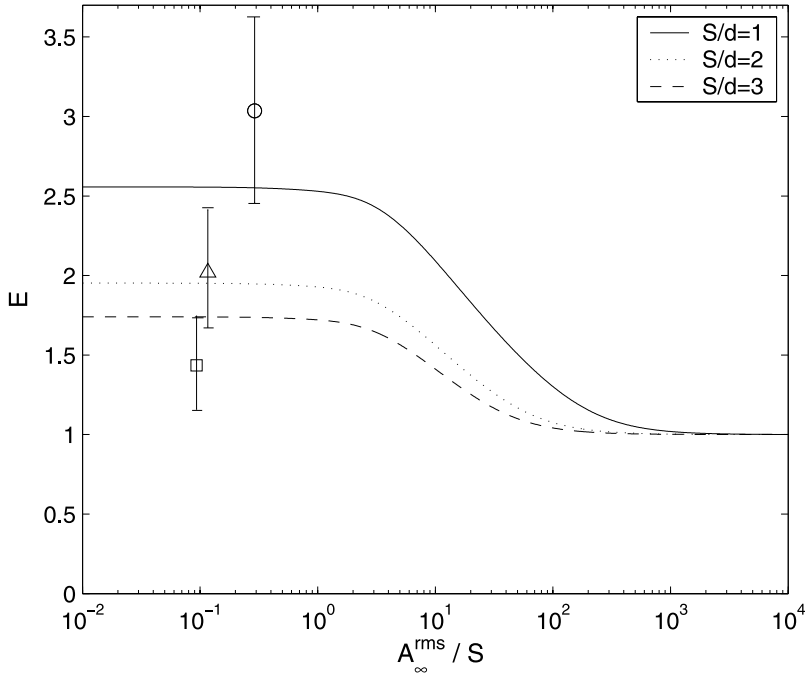

Figure 8. Predicted curves of oscillatory flow mass transfer enhancement E as a function of the wave orbital excursion length A_∞^{rms}, using results from the canopy flow model described in the work of LKM1, Figure 4. Data of measured E are plotted from Figure 7, where each data point represents the mean value of A_∞^{rms} at that spacing.

canopy geometry and can vary greatly between unidirectional and oscillatory flow.

[33] By combining the flow model in the work of LKM1 with the mass transfer model developed in this paper, it is possible to investigate oscillatory mass transfer enhancement within different canopies experiencing different flow conditions. As an example let us consider the problem of mass transfer from coral reef canopies. In section 5 of LKM1, the flow inside these coral canopies was estimated under a range of different wave conditions [see LKM1, Table 4] and these results can be directly applied to investigate rates of mass transfer from these canopies. For each coral species the ratio α_i/α_c was calculated and thus $E_{\max}$ can be estimated using equation (28), as listed in Table 3. The ratio α_w/α_c was also calculated for each coral for three different wave excursion lengths A_∞^{rms} = 1, 10 and 100 cm, and these results can be used with equation (27) to determine E for each wave condition (Table 3). The theoretical maximum enhancement $E_{\max}$ for these corals averages roughly 3 and the actual enhancement E decreases to as low as 1.8 as A_∞^{rms} is increased. It is interesting to note that *Reidenbach et al.* [2005] directly measured E in the three coral species listed in Table 3, and observed values between 1.6 and 2.9, of similar magnitude to the predicted enhancement. Oscillatory flow is thus expected to significantly increase rates of nutrient mass transfer to these reef communities.

[34] The mass transfer model developed in section 2, based on the in-canopy flow speed, worked well to predict mass transfer rates for cases where the flow was either unidirectional or oscillatory. However, there are certain situations where assumptions inherent to the model are likely not valid and hence the model may not give accurate mass transfer predictions. For example, the model was derived using an empirical formula which describes mass transfer for two-dimensional flow around a circular cylinder. This model may not be appropriate when flow around the canopy elements is highly three-dimensional, i.e., for sparse canopies where λ_f is small such that the shear-layer at the top of the canopy penetrates all the way down to the bed [*Coceal and Belcher*, 2004]. For dense canopies, with relatively large λ_f, the shear-layer is confined to a thin region near the top of the canopy and the flow is mostly two-dimensional below this region. In the work of LKM1, the thickness of this shear layer was found to be roughly 10–20% of the total canopy depth [see LKM1, Figure 8], so for the range of geometries used in the experiments, the two-dimensional flow assumption is reasonable.

[35] Moreover, our model is based on a unidirectional mass transfer formula and is extended to oscillatory canopy flows by replacing the unidirectional velocity in the original formula with the rms oscillatory flow velocity. This assumption may not necessarily be justifiable a priori, since it is possible that the mass transfer process is modified by the unsteady nature of the oscillatory flow. Nonetheless, our results clearly showed that, for the canopies and flow conditions used in these experiments, the unidirectional mass transfer formula in equation (4) can be used to describe mass transfer for oscillatory flows if the measured in-canopy oscillatory flow speed was used.

[36] Results from our experiments confirm that the specific morphology of the canopy influences mass transfer rates, which has important biological implications. For unidirectional flow, mass transfer from an individual canopy element was found to decrease significantly as the element spacing decreased, due to sheltering from upstream ele-

Table 3. Modeled Oscillatory Flow Mass Transfer Enhancement for Branched Reef Corals[a]

Source	Coral Species	E_{max}	E for A_∞^{rms} = 1 cm	10 cm	100 cm
Chamberlain and Graus [1975]	Oculina diffusa	2.6	2.6	2.4	1.7
	Seriatopora hysterix	3.4	3.4	2.8	1.8
Lesser et al. [1994]	Pocillopora damicornis	3.2	3.2	2.7	1.8
Marshall [2000]	Acropora formosa	3.2	3.2	2.7	1.8
	Acropora humilis	2.9	2.9	2.6	1.8
	Acropora palifera	2.6	2.6	2.4	1.7
	Pocillopora damicornis	3.2	3.2	2.7	1.8
	Porites cylindrica	3.0	3.0	2.6	1.8
	Seriatopora hystrix	4.2	4.0	3.0	1.8
	Stylophora pistillata	3.2	3.2	2.7	1.8
Reidenbach et al. [2005]	Stylophora pistillata	3.0	3.0	2.6	1.8
	Pocillopora verrucossa	3.1	3.0	2.7	1.8
	Porites compressa	3.0	3.0	2.6	1.8

[a]From LKM1 (Table 4).

ments. If this canopy element was, for example, an individual organism such as a bivalve, the flux of a scalar to the organism would be reduced as the organism spacing decreased. This is consistent with conclusions by *Helmuth et al.* [1997], that the rate of mass flux to an individual organism is significantly reduced when the organism is living in a densely packed aggregation compared to living in isolation. Similarly, *Reidenbach et al.* [2005] compared measurements for corals of the same species but having different branch spacings and found that mass transfer rates measured between the branches were lowest from corals of that species with the tightest branch spacings. Therefore the specific morphology of the canopy (aggregation) has a significant influence on the flux of a scalar to an individual organism (or single canopy branch), which is confirmed by the observations in these experiments.

[37] When the canopy is viewed in its entirety, however, the mass transfer rate per unit canopy plan area was found to increase as the canopy element spacing decreased, because the total surface area of the canopy was subsequently higher. As a result, although a canopy element such as a single coral branch may experience a reduced mass flux when the canopy density increases, the canopy as whole (e.g., the entire coral colony), would experience a higher total mass flux when the density increases. For colonial organisms that have the ability to share nutrients, a dense canopy would thus be ideal, since the overall flux of the scalar to the colony is highest when the canopy elements are densest. Hence for benthic communities that want to maximize nutrient mass transfer, a sparse canopy is optimum for an individual organism (element) in a canopy composed of neighboring organisms, while a dense canopy is ideal for an organism which itself forms the canopy.

[38] Although the model canopies used in this study are far simpler than complex natural canopies found in the environment, the ideas developed in this paper can help to understand relevant biological-physical interactions in these complex systems. Studies discussed in the introduction have found that surface waves enhance nutrient uptake to benthic canopies formed by, for example, seagrasses [*Thomas and Cornelisen*, 2003] and rates of nitrogen fixation in turf algae [*Williams and Carpenter*, 1998], compared to a unidirectional flow of the same magnitude. This is consistent with the findings in this paper, where it was determined that an oscillatory flow generates a higher in-canopy flow which in turn results in higher mass transfer rates. Oscillatory flow thus has the ability to greatly increase the rate at which canopy-forming organisms can take up nutrients, and thus compared to unidirectional flow, surface wave motion clearly has the potential to significantly enhance the productivity of benthic organisms.

Appendix A: Estimating $\widehat{C}_{max}$

[39] A key assumption in the canopy mass transfer model in section 2 is that the solute released by each canopy element does not build up to a significant concentration inside the canopy, i.e., $\widehat{C}_{max} \ll C_o$ where $\widehat{C}_{max}$ is the maximum in-canopy concentration and C_o is the wall concentration. If the in-canopy concentration $\widehat{C}(x)$ becomes comparable to C_o, the mass transfer coefficient $\widehat{\beta}_e$ will be reduced per equation (1) due to the reduced concentration gradient at the element surface. In the experiments described in this paper, $\widehat{C}(x)$ was not measured directly. It is shown here, however, that this concentration is expected to be orders of magnitude smaller than C_o in these experiments such that $\widehat{C}$ in equation (6) can effectively be ignored.

[40] To estimate $\widehat{C}_{max}$, a control volume approach is implemented. Consider the control volume formed by a repeating canopy element unit of plan area A_T (Figure 3). This control volume is highlighted in Figure A1. The goal of this calculation is to determine the value $\widehat{C}_{max}$ for the range of flow conditions used in these experiments. This concentration is expected to be highest in the unidirectional flow experiments where the scalar is most "trapped" inside the canopy [*Nepf and Vivoni*, 2000], since oscillatory flow is expected to increase vertical mixing in the canopy and result in lower in-canopy concentrations [*Reidenbach*, 2004]. As a result, in this analysis the unidirectional flow case is considered.

[41] The unidirectional flow velocity in the canopy (denoted $\widehat{U}_c$) is attenuated from the free-stream current velocity $U_{\infty,c}$. Consider now the case where $\widehat{U}_c$ is fully developed but there is a sudden presence of gypsum canopy elements at some downstream distance x_g. Downstream of x_g the in-canopy concentration $\widehat{C}(x)$ is expected to increase as the solute is released from the gypsum cylinders. At some distance downstream, $\widehat{C}$ attains a constant maximum value

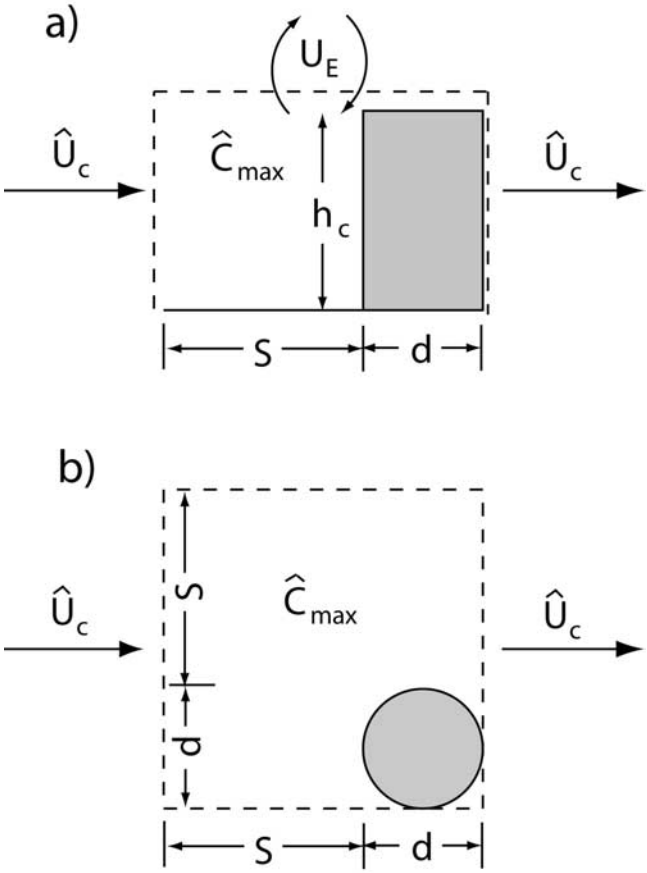

Figure A1. Mass balance in a repeating canopy element unit: (a) side view and (b) plan view.

$\widehat{C}_{\max}$, which occurs when the mass exchanged with the water column at the top of the canopy is balanced by the mass released by the canopy elements. When this occurs $\widehat{C}$ is fully developed and reflects the maximum possible concentration $\widehat{C}_{\max}$ inside a canopy for a given unidirectional flow condition and canopy geometry.

[42] Now consider a mass balance over the control volume illustrated in Figure A1. When the in-canopy velocity and concentration field is fully developed, the mass per unit time released into the canopy is $\widehat{F}_e A_e$ and this is equal to the mass per unit time exchanged between the in-canopy and above-canopy flows. This exchange process has been described using a vertical exchange velocity U_E at the top of the canopy ($z = h_c$) [*Bentham and Britter*, 2003]. A mass balance in the control volume then gives

$$\widehat{F}_e A_e = U_E \widehat{C}_{\max} A_T. \tag{A1}$$

Substituting equation (6) for $\widehat{F}_e$ into equation (A1) and rearranging gives

$$\frac{\widehat{C}_{\max}}{C_o} = \frac{1}{(U_E A_T)/\left(\widehat{\beta}_e A_e\right) + 1} = \frac{1}{(U_E/\beta_{can}) + 1}, \tag{A2}$$

where β_{can} was related to $\widehat{\beta}_e$ by equation (15). In order to estimate $\widehat{C}_{\max}$ using equation (A2), the exchange velocity U_E must be estimated. *Bentham and Britter* [2003] describe a model to predict U_E in canopies for unidirectional flow and find

$$U_E = \frac{u_{*c}^2}{U_{\infty,c} - \widehat{U}_c}, \tag{A3}$$

where u_{*c} is the friction velocity based on the canopy shear stress. We are interested in the maximum value of $\widehat{C}_{\max}/C_o$ which will occur in experiments where from equation (A2) U_E is smallest. This will occur from equation (A3) when $U_{\infty,c}$ is weakest and the cylinder density is highest (since $\widehat{U}_c/U_{\infty,c}$ is smallest in this case). For the experiments with the weakest flow, $U_{\infty,c}$ was approximately 0.05 m/s. Using results from LKM1, at the densest cylinder spacing ($S/d = 1$), $\widehat{U}_c/U_{\infty,c} \approx 0.1$ and $u_*/U_{\infty,c} \approx 0.1$. Thus for these flow conditions U_E takes a minimum value in the experiments of 0.006 m/s. In these experiments the maximum value of $\widehat{\beta}_e$ was approximately 1×10^{-5} m/s. Substituting these values into equation (A2) gives the maximum value of $\widehat{C}_{\max}$ expected in these experiments:

$$\frac{\widehat{C}_{\max}}{C_o} \approx 0.003. \tag{A4}$$

The maximum in-canopy concentration $\widehat{C}_{\max}$ in all experiments is estimated here to be three orders of magnitude smaller than C_o and hence can be ignored.

Notation

A_e	canopy element surface area.
A_T	area of repeating canopy element unit.
A_∞^{rms}	wave orbital excursion length.
C_{ref}	reference concentration.
C_0	surface concentration.
C_∞	concentration in bulk fluid.
$\widehat{C}$	vertically averaged canopy concentration.
d	cylinder diameter.
D	molecular diffusivity of solute.
D_{CaSO4}	effective diffusivity of $CaSO_4$.
E	mass transfer enhancement factor due to waves.
$E_{\max}$	maximum value of E for a given canopy.
f	empirical function describing mass transfer.
F	mass flux.
g	function describing canopy geometry.
h_c	canopy height.
Re_e	Reynolds number.
S	canopy element spacing.
Sc	Schmidt number.
Sh_e	Sherwood number.
St_e	Stanton number.
T	wave period.
U_c	current velocity profile.
U_E	vertical canopy exchange velocity.
U_w	phase-varying oscillatory velocity profile.
$\widehat{U}_s$	average flow speed inside canopy.
u_*	friction velocity.
W_g	molecular weight of gypsum.
z	vertical elevation from canopy base.

α_c	unidirectional canopy flow attenuation parameter.
α_i	attenuation parameter for inertia dominated flow.
α_w	oscillatory canopy flow attenuation parameter.
β	local mass transfer coefficient.
β_{can}	mass transfer coefficient for canopy array.
β_e	canopy-element mass transfer coefficient.
ΔM	total gypsum mass loss from canopy element.
$\Delta M'$	gypsum mass loss before correction.
Δt	experiment duration.
λ_f	frontal area canopy geometry parameter.
λ_p	plan area canopy geometry parameter.
ν	kinematic viscosity of water.
Subscripts	
c	parameter associated with current.
w	parameter associated with oscillatory flow.
Superscripts	
rms	root mean squared velocity (rms).
Other	
$\wedge$	overhat denoting canopy depth-averaged velocity.

[43] **Acknowledgments.** We thank two anonymous reviewers for providing helpful comments that improved the manuscript. Support for this project by the National Science Foundation under grant OCE-0117859 is gratefully acknowledged.

References

Atkinson, M. J., and R. W. Bilger (1992), Effect of water velocity on phosphate uptake in coral reef-flat communities, *Limnol. Oceanogr.*, *37*, 273–279.

Baird, M. E., and M. J. Atkinson (1997), Measurement and prediction of mass transfer to experimental coral reef communities, *Limnol. Oceanogr.*, *42*(8), 1685–1693.

Barlow, J. F., I. N. Harman, and S. E. Belcher (2004), Scalar fluxes from urban street canyons. Part I: Laboratory simulation, *Boundary Layer Meteorol.*, *113*(3), 369–385.

Bentham, T., and R. Britter (2003), Spatially averaged flow within obstacle arrays, *Atmos. Environ.*, *37*(15), 2037–2043.

Bilger, R. W., and M. J. Atkinson (1992), Anomalous mass transfer of phosphate on coral reef flats, *Limnol. Oceanogr.*, *37*(2), 261–272.

Carpenter, R. C., J. M. Hackney, and W. H. Adey (1991), Measurements of primary productivity and nitrogenase activity of coral-reef algae in a chamber incorporating oscillatory flow, *Limnol. Oceanogr.*, *36*(1), 40–49.

Chamberlain, J. A., and R. R. Graus (1975), Water-flow and hydromechanical adaptations of branched reef corals, *Bull. Mar. Sci.*, *25*(1), 112–125.

Churchill, S. W., and M. Bernstein (1977), Correlating equation for forced-convection from gases and liquids to a circular-cylinder in cross-flow, *J. Heat Transfer Trans. ASME*, *99*(2), 300–306.

Coceal, O., and S. Belcher (2004), A canopy model of mean winds through urban areas, *Q. J. R. Meteorol. Soc.*, *130*, 1349–1372.

Falter, J. L., M. Atkinson, and C. Coimbra (2005), Effects of surface roughness and oscillatory flow on the dissolution of plaster forms: Evidence for nutrient mass transfer to coral reef communities, *Limnol. Oceanogr.*, *50*(1), 246–254.

Finnigan, J. (2000), Turbulence in plant canopies, *Ann. Rev. Fluid Mech.*, *32*, 519–571.

Harman, I. N., J. F. Barlow, and S. E. Belcher (2004), Scalar fluxes from urban street canyons. Part II: Model, *Boundary Layer Meteorol.*, *113*(3), 387–409.

Helmuth, B. S. T., K. P. Sebens, and T. L. Daniel (1997), Morphological variation in coral aggregations: Branch spacing and mass flux to coral tissues, *J. Experiment. Mar. Biol. Ecol.*, *209*(1–2), 233–259.

Kays, W. M., and M. E. Crawford (1993), *Convective Heat and Mass Transfer*, *Ser. in Mech. Eng.*, 3rd ed., McGraw-Hill, New York.

Lerman, A. (1979), *Geochemical Processes Water and Sediment Environments*, John Wiley, Hoboken, N. J.

Lesser, M. P., V. M. Weis, M. R. Patterson, and P. L. Jokiel (1994), Effects of morphology and water motion on carbon delivery and productivity in the reef coral, Pocillopora-damicornis (Linnaeus)—Diffusion-barriers, inorganic carbon limitation, and biochemical plasticity, *J. Exper. Mar. Biol. Ecol.*, *178*(2), 153–179.

Li, Y., and S. Gregory (1974), Diffusion of ions in sea water and deep-sea sediments, *Geochim. Cosmochim. Acta*, *38*, 703–714.

Lide, D. (Ed.) (2003), *CRC Handbook of Chemistry and Physics*, 84th ed., CRC Press, Boca Raton, Fla.

Lowe, R. J., J. R. Koseff, and S. G. Monismith (2005), Oscillatory flow through submerged canopies: 1. Velocity structure, *J. Geophys. Res.*, *110*, C10016, doi:10.1029/2004JC002788.

Marshall, P. A. (2000), Skeletal damage in reef corals: relating resistance to colony morphology, *Mar. Ecol. Prog. Ser.*, *200*, 177–189.

Nepf, H. M. (1999), Drag, turbulence, and diffusion in flow through emergent vegetation, *Water Resour. Res.*, *35*(2), 479–489.

Nepf, H. M., and E. R. Vivoni (2000), Flow structure in depth-limited, vegetated flow, *J. Geophys. Res.*, *105*(C12), 28,547–28,557.

Patterson, M. R., K. P. Sebens, and R. R. Olson (1991), Insitu measurements of flow effects on primary production and dark respiration in reef corals, *Limnol. Oceanogr.*, *36*(5), 936–948.

Porter, E. T., L. P. Sanford, and S. E. Suttles (2000), Gypsum dissolution is not a universal integrator of "water motion," *Limnol. Oceanogr.*, *45*(1), 145–158.

Reidenbach, M. (2004), Mixing and mass transfer in the turbulent boundary layer of coral reefs, Ph.D. thesis, Stanford Univ., Stanford, Calif.

Reidenbach, M. A., J. R. Koseff, S. G. Monismith, J. V. Steinbuck, and A. Genin (2005), The effects of waves and morphology on mass transfer within branched reef corals, *Limnol. Oceanogr.*, in press.

Sanford, L. P., and S. M. Crawford (2000), Mass transfer versus kinetic control of uptake across solid-water boundaries, *Limnol. Oceanogr.*, *45*(5), 1180–1186.

Sebens, K. P., B. Helmuth, E. Carrington, and B. Agius (2003), Effects of water flow on growth and energetics of the scleractinian coral Agaricia Tenuifolia in Belize, *Coral Reefs*, *22*(1), 35–47.

Stumm, W., and J. Morgan (1996), *Aquatic Chemistry: Chemical Equilibria and Rates in Natural Waters*, 3rd ed., John Wiley, Hoboken, N. J.

Thomas, F. I. M., and C. D. Cornelisen (2003), Ammonium uptake by seagrass communities: effects of oscillatory versus unidirectional flow, *Mar. Ecol. Prog. Ser.*, *247*, 51–57.

Thomas, F. I. M., C. D. Cornelisen, and J. M. Zande (2000), Effects of water velocity and canopy morphology on ammonium uptake by seagrass communities, *Ecology*, *81*(10), 2704–2713.

Thompson, T. L., and E. P. Glenn (1994), Plaster standards to measure water motion, *Limnol. Oceanogr.*, *39*(7), 1768–1779.

White, B., and H. M. Nepf (2003), Scalar transport in random cylinder arrays at moderate reynolds number, *J. Fluid Mech.*, *487*, 43–79.

Williams, S. L., and R. C. Carpenter (1998), Effects of unidirectional and oscillatory water flow on nitrogen fixation (acetylene reduction) in coral reef algal turfs, Kaneohe Bay, Hawaii, *J. Experiment. Mar. Biol. Ecol.*, *226*(2), 293–316.

Zukauskas, A., and J. Ziugzda (1985), *Heat Transfer of a Cylinder in Crossflow, Experiment. and Appl. Heat Transfer Guide Books*, Taylor and Francis, Philadelphia, Pa.

J. L. Falter, Hawaii Institute of Marine Biology, University of Hawaii, P.O. Box 1346, Kaneohe, HI 96744, USA. (falter@hawaii.edu)

J. R. Koseff, R. J. Lowe, and S. G. Monismith, Environmental Fluid Mechanics Laboratory, Department of Civil and Environmental Engineering, Stanford University, Terman Building, Room M-29, Stanford, CA 94305-4020, USA. (koseff@stanford.edu; rlowe@stanford.edu; monismith@stanford.edu)